

Underwater Energy Harvesting and Sensing by Sweeping Out the Charges in an Electric Double Layer using an Oil Droplet

Huaifang Qin, Liang Xu,* Shiquan Lin, Fei Zhan, Kai Dong, Kai Han, Huamei Wang, Yawei Feng, and Zhong Lin Wang*

As an emerging technology for energy harvesting and distributed power supply, triboelectric nanogenerators are mainly based on a dielectric capacitive structure. Here, a new mechanism by introducing an oil phase into a water–solid interface is demonstrated for energy harvesting based on electric double layer (EDL) capacitance. Through squeezing and releasing oil droplets on a dielectric surface in water environment, charge transfer is observed in the back electrode accompanying the movement of the oil–water–solid three-phase line. The charge transfer is mainly attributed to the effect that the oil phase sweeps away ions near the dielectric surface in the EDL due to the discrepancy of EDL between water–solid and oil–solid interfaces. Under the water environment, the device is shown to be capable of direct energy harvesting and self-powered sensing without costly packaging. As a new working mode relying on EDL, it allows developing nanogenerators adaptive to severe environments even underwater with low friction and wear, and narrowing the gap between energy harvesting devices and electro-chemical devices. Through further enhanced EDL, it is reasonable to anticipate devices with an ultrahigh charge density comparable with EDL super capacitors, opening up an avenue toward new nanogenerators with overwhelming performance for practical applications ranging from blue energy harvesting to electro-catalysis.

1. Introduction

The development of the Internet of Things (IoT), wearable electronics and robotics has put forward new requirements for the power supply.^[1] Mobility, maintenance-free, and environment-friendliness are some desired characteristics. As an emerging energy-harvesting technology, the triboelectric nanogenerator (TENG, also called Wang generator) can efficiently convert mechanical energy into electricity based on the coupling of triboelectrification and electrostatic induction.^[2] Its theoretical fundamental can be derived from the Maxwell's displacement current.^[1e] Compared with other energy-harvesting approaches, TENGs exhibit merits of low cost, light weight, easy fabrication, and rich material choices.^[1e,2a,b,d] It can effectively harvest ubiquitous mechanical energy in the environment, even for irregular low-frequency motions, such as wind, rain drop, water wave, human motion, and so on.^[3] Therefore, it is regarded as a promising solution for sustainable in situ power supply and self-powered systems.

The operation of TENGs classically relies on contact electrification (or triboelectrification) to generate two charged surfaces, at least one of which is an insulated surface.^[4] The two layers of charges on the surfaces separated by dielectrics (typically air) exhibit a structure similar to a dielectric capacitor, and a capacitive model has been used to analyze the output characteristics of TENGs successfully.^[5] Due to the relative low capacitance of the structure, the achievable charge density is limited, because higher charge density will cause dielectric breakdown.^[6] As a critical parameter, the low charge density severely limits the output power of TENGs.^[7] The device is also sensitive to humidity, and its performance will degrade seriously in moisture.^[8] Thus packaging is highly required in damp environment or underwater. Due to the difficulty of maintaining reliable packaging for a long time, it is challenging to apply the device in water environment, though there are enormous demands in blue energy harvesting and self-powered sensing in ocean.^[9] Meanwhile, the contact surface always suffers from abrasion and heat generation, although liquid droplets can be

H. Qin, L. Xu, S. Lin, F. Zhan, K. Dong, K. Han, H. Wang, Y. Feng, Z. L. Wang
Beijing Institute of Nanoenergy and Nanosystems
Chinese Academy of Sciences
Beijing 101400, P. R. China
E-mail: xuliang@binn.cas.cn

H. Qin, L. Xu, S. Lin, F. Zhan, K. Dong, K. Han, H. Wang, Y. Feng, Z. L. Wang
School of Nanoscience and Technology
University of Chinese Academy of Sciences
Beijing 100049, P. R. China

Z. L. Wang
CUSTech Institute of Technology
Wenzhou, Zhejiang 325024, P. R. China
E-mail: zlwang@binn.cas.cn

Z. L. Wang
School of Materials Science and Engineering
Georgia Institute of Technology
Atlanta, GA 30332-0245, USA

 The ORCID identification number(s) for the author(s) of this article can be found under <https://doi.org/10.1002/adfm.202111662>.

DOI: 10.1002/adfm.202111662

adopted as one tribo-material to suppress surface wear in some situations.^[3b,10]

Distinguished from dielectric capacitance, electric double layer (EDL) is another capacitive structure which forms at the liquid–solid interfaces mainly involving electrons in the solid surface and ions in the liquid.^[11] It enables EDL super capacitors which have much larger capacitance than dielectric capacitors.^[11e,12] Inspired by the capacitive feature of classical TENGs similar to dielectric capacitance, it can be expected that devices based on EDL may present a series of novel characteristics, opening up new possibilities and paradigm shift for developing high-performance energy-harvesting devices. However, unlike the static charges bound at solid surfaces in classical TENGs, it is challenging to effectively drive the ions to move in the EDL due to the fluidity, which is required to deliver mechanical energy from external agitations to the ions and conduct energy conversion.

In this work, a mechanism by introducing oil phase into water–solid interface is demonstrated to enable a nanogenerator based on EDL (referred as EDL-NG). Through squeezing and releasing oil droplets on a dielectric surface in water environment, charge transfer is observed in the back electrode accompanying the spread and retraction of the oil droplet and the movement of oil–water–solid three-phase line. Such charge transfer is mainly attributed to the effect that the oil phase sweeps away ions near the dielectric surface in the EDL due to the discrepancy of EDL between water–solid and oil–solid interfaces. The characteristics of the device is investigated in details, which is still effective in various aqueous environment, and can be further enhanced by charge pre-implantation in the dielectric surface. Without costly packaging, the device is shown to be capable of direct energy harvesting and self-powered sensing underwater. The EDL-NG reveals that the charges in the EDL can be effectively driven for energy harvesting with oil phase, narrowing the gap between energy harvesting devices and electro-chemical devices. As a new working mode relying on EDL, it allows developing nanogenerators with low friction and wear, and adaptability to severe environments even underwater. Through further enhanced EDL, it is reasonable to anticipate devices with an ultrahigh charge density comparable with super capacitors, opening up an avenue toward super nanogenerators with overwhelming performance for practical applications ranging from blue energy harvesting to electro-catalysis.

2. Results and Discussion

2.1. Structure and Working Principle

The principal structure of the device is shown in **Figure 1a**. An oil droplet (typically squalene) is placed upon a dielectric layer (typically polytetrafluoroethylene, PTFE), with a back electrode (copper) wrapped between the dielectric layer and a substrate, forming the lower plate. A bare inert electrode (platinum, Pt) is connected to the back electrode through an external circuit or a load and exposed to the environment. The whole structure is immersed in water, while the oil droplet is squeezed and released periodically in vertical direction by an upper

plate (typically glass with PTFE film attached) during operation. The dielectric surface is electrified through triboelectrification, which will attract counter ions in water and forms EDL at the water–solid interface. The EDL typically can be described by the Stern-Grahame EDL model (Figure S1, Supporting Information),^[11c,13] and details of the model is presented in Note S1, Supporting Information. With the spread of the oil droplet during squeezing, the position occupied by water will be gradually replaced by oil, and the attracted counter ions in the EDL will be swept away from the surface with water, leaving the charges on the solid surface unshielded, which induces electric potential variation in the back electrode due to electrostatic induction. By subsequently releasing the oil droplet, it will retract and water will occupy previous position again and the EDL restores. Such process is schematically shown in Figure 1b, and it is supported by the fact that there are very few ions in the oil phase. Detailed theoretical discussion based on the EDL model is presented in Note S2, Supporting Information.^[14]

Figure 1c further demonstrates the working mechanism of the EDL-NG, and the EDL is schematically simplified as a few pairs of negative charges on the solid surface and shielding cations in the water. By pushing the upper plate down, the oil droplet will be squeezed vertically and spread on the dielectric surface, sweeping away charges in the EDL (Figure 1c-II). The unshielded negative charges on the dielectric surface will induce charge transfer between the two electrodes, and electrons will flow to the bare electrode which attract cations in the water, leaving positive charges in the back electrode. As the upper plate moves upward, the spread oil droplet gradually retracts (Figure 1c-IV). The position occupied by the oil is replaced by the water, and the cations will be attracted to the dielectric surface again, shielding the negative surface charges. Thus, the electrons in the bare electrode will flow back, generating a signal opposite to squeezing the oil droplet. Through repeatedly squeezing and releasing the oil droplet, an alternate current can be observed in the external circuit. Here, the wetting and dewetting process of the oil droplet is mainly determined by the geometry change of the oil droplet under squeezing and releasing of the upper plate.

A proof-of-principle device was fabricated to validate the working mechanism. The detailed structure of the device is shown in Figure S2, Supporting Information, and more details on the fabrication procedures of the device are provided in the Experimental Section. A PTFE dielectric layer and a squalene droplet were adopted here, and the upper plate was fabricated by attaching a PTFE layer on a glass substrate. As shown in Figure 1d and Video S1, Supporting Information, there will be no charge transfer observed in the external circuit during moving down of the oil until it contacts the lower dielectric surface, indicating that the output is not likely to be caused by charges in the oil droplet. After contacting, by further pushing the upper plate downward, the oil droplet gradually spreads on the surface to replace the water. As the area of oil–solid interface increases, the amount of transferred charges also rises until the squeezing stops. Then, with upward moving of the upper plate, the oil droplet retracts and the oil–solid interface shrinks, resulting in reversed charge transfer.

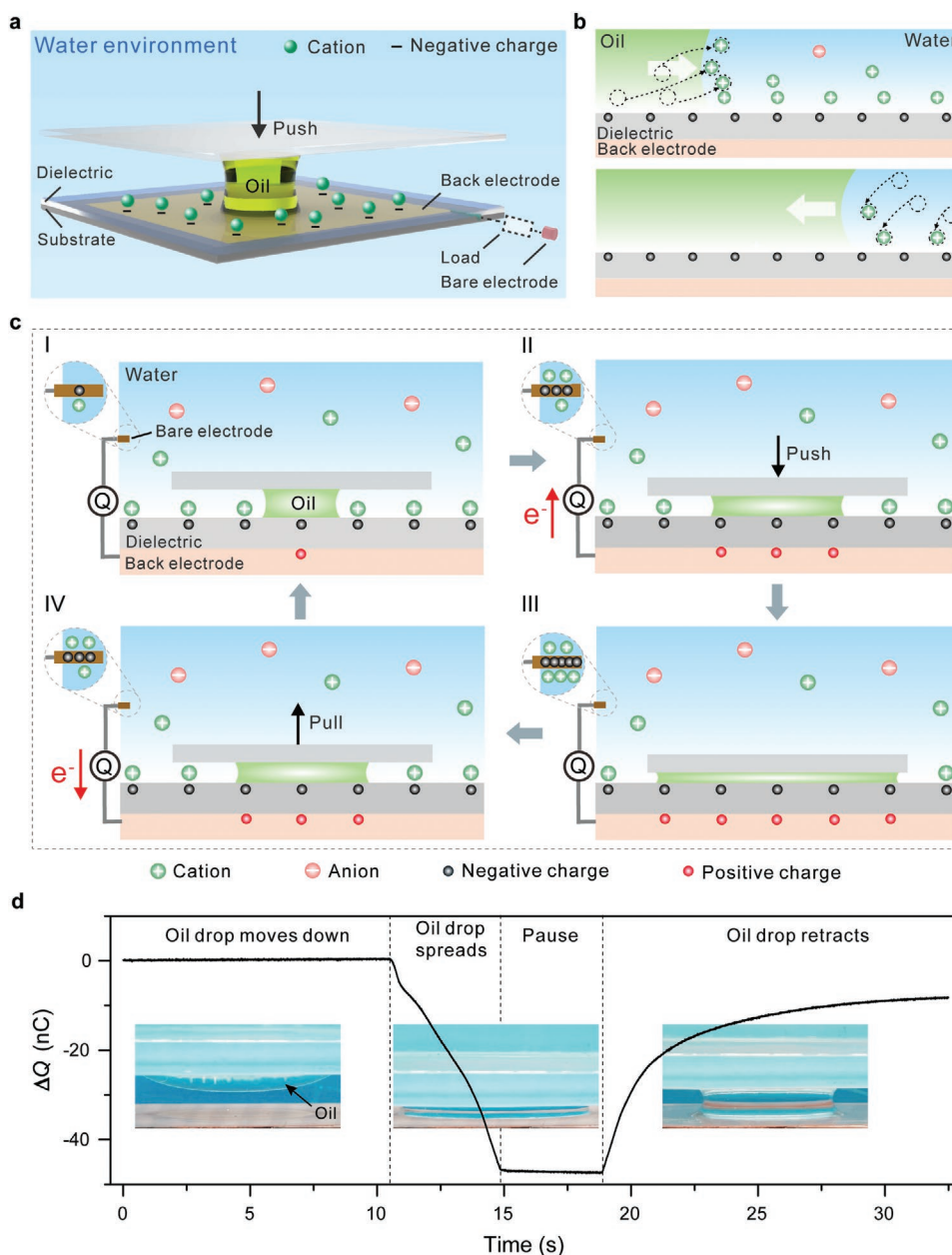


Figure 1. Device structure and working principle. a) Principal structure of the device. b) Schematic of spread and retraction of oil at the interface. c) Working mechanism of the EDL-NG. d) Charge transfer of the EDL-NG in operation. Inset: states of the oil droplet.

2.2. Output Characteristics in Deionized Water

The basic electrical output characteristics of the device was further investigated systematically in deionized (DI) water. Firstly, the output of the device with or without oil (squalene, aladdin) trapped upon the dielectric surface is compared (Figure S3, Supporting Information). The volume of the oil droplet used in the experiment is 0.9 mL unless otherwise specified. **Figure 2a–c** present the transferred charges (ΔQ), short-circuit current (I_{SC}) and open-circuit voltage (V_{OC}) of the two situations. As the upper plate maintains an agitation frequency of 0.12 Hz, with oil trapped, ΔQ , I_{SC} and V_{OC} of 25.6 nC,

35 nA and 43.1 V are obtained respectively under a variation of oil–solid contact area of 16 cm², and the signals vanish totally without the oil droplet. **Figure 2d** compares the transferred charges of three situations: the lower plate contacting with a copper electrode, the device submerged in water from air, and squeezing the oil to fully cover the interface, which have outputs of 14.4, 25.6, and –26.6 nC, respectively. The results show that the liquid contact allows larger charge transfer than solid contact due to a better contact state.

Figure 2e shows the relationship between the transferred charges and the variation of the oil–solid contact area (see **Figure S4** and **Note S3**, Supporting Information). The absolute

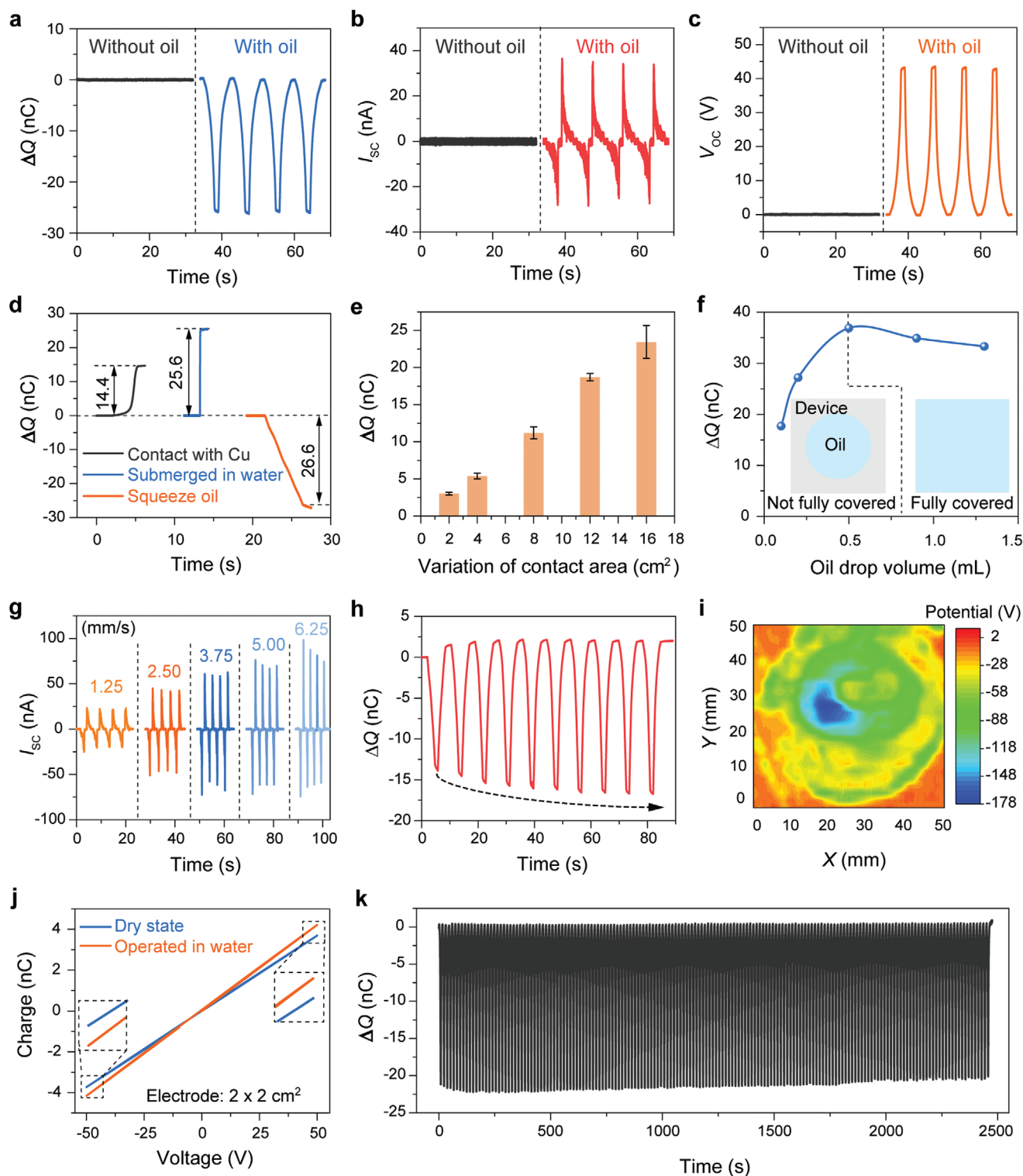


Figure 2. Output characteristics of the device in deionized water. a–c) Transferred charges (a), short-circuit current (b), and open-circuit voltage (c) of the device with and without oil trapped upon the dielectric surface. d) Transferred charges of three situations. e) Dependence of transferred charges on variation of oil–solid contact area. f) Transferred charges of the device with different volumes of oil. Inset: schematic diagram of oil droplet spreading on dielectric surface. g) Dependence of short-circuit current on the speed of squeezing oil. h) Transferred charges in the initial stage. i) Surface potential distribution on the dielectric surface with oil squeezed. j) Charge–voltage relation in the capacitance test. k) Transferred charges of the device with long-term operation.

value of transferred charges increases almost linearly with the variation of the contact area. The influence of the oil drop volume on the output is shown in Figure 2f. With the upper plate pushed to contact the lower plate to squeeze the oil drop to the largest degree, a 0.5 mL oil droplet is enough to fully cover the whole interface, and an absolute value of charge output of about 36.9 nC is obtained (Details are shown in Figure S5, Supporting Information). When the oil drop volume is larger than 0.5 mL, the variation of contact area decreases due to the increase of initial contact area (Figure S5c, Supporting Information), which leads to the decrease of transferred charges. Figure 2g presents the relationship between the I_{SC} and the speed of squeezing oil. With rising speed from 1.25 to 6.25 mm s⁻¹, the output current also increases almost linearly from 23.2 to 98.4 nA under a variation of oil–solid contact area of 16 cm².

Figure 2h shows the transferred charges of squeezing oil droplet in the initial stage. As the number of cycle rises, the transferred charges gradually increase and finally reach saturation, which should be attributed to the enhancement of the surface charges on the dielectric surface due to triboelectrification with the oil droplet. Generally, more static charges on the dielectric surface will attract more ions in water, and the oil can sweep out more ions which produce larger output. To verify the result, the surface potential distribution after squeezing oil to different extents were tested, using a scanning method shown in Figure S6, Supporting Information. Compared with the initial surface potential distribution (Figure S6b, Supporting Information), a circular potential distribution is formed on the surface after squeezing oil for 160 cycles and 100 cycles to two different contact areas (Figure 2i), and the inner potential with oil contact is lower than the surrounding potential that is still consistent with initial surface potential. Considering that the surface potential is closely related to the charge distribution,^[15] triboelectrification between the oil droplet and the dielectric surface of the device can be confirmed.

In addition, to investigate whether the oil droplet can completely exclude water at the interface, the capacitances in dry oil state and underwater operated state are compared by replacing the upper plate with a copper electrode. Here, the capacitance forms between the back electrode and the upper copper electrode that squeezes the oil and contacts with the lower plate. The squeezed oil and the PTFE layer between the two electrodes play the role of dielectric materials, and if water is not completely excluded after squeezing the oil underwater, the capacitance should be affected. The capacitance (C) measurement was conducted by injecting charges (Q) into the electrodes using certain voltage (V) based on the relationship $C = Q/V$. Details of the experiment can be found in Figure S7 and Note S4, Supporting Information. As shown in Figure 2j, after operating in water, the capacitance tested is slightly larger than the original dry state, implying that the interface may be changed which could be residual water or ions with higher dielectric constant, although bulk water has been excluded by the squeezed oil.

Long-term operation of the device was also tested, as shown in Figure 2k. In the initial stage, the transferred charges (variation of contact area: 16 cm²) gradually increase to reach saturation, then the output keeps relatively stable in long-term cycles.

2.3. Influence of Solutions, Dielectric Materials and Oils

The output characteristics of the device in different solutions are studied in details, as shown in Figure 3a–d. The volume of the oil droplet used in the experiment is 0.9 mL, and the variation of contact area is 8 cm² unless otherwise specified. Firstly, as shown in Figure 3a, the effect of different concentrations of NaCl solutions on the transferred charges is studied. When the concentration of the NaCl solution increases from 0 to 0.5 mol L⁻¹, the transferred charges only decrease from 12.55 to 11.37 nC. Thus, the output is not quite sensitive to the concentration in the range covered by the experiment.

Figure 3b shows the results with different solutions, and the charge output is normalized via dividing by the transferred charges in DI water for better comparison. The concentration of the solutions is uniformly 0.5 mol L⁻¹ (close to 35‰ salinity of sea water). With different solutions, the normalized charges are all below 1, which implies a decrease in the charge output relative to DI water. As the anion valence increases, the degree of attenuation becomes more obvious. The normalized charge output in Na₃PO₄ solution is reduced to about 1/3, which could be attributed to the anion PO₄³⁻. The high valence of the ion possibly induces stronger interaction of the ion with the surface which cannot be easily swept away by the oil. Meanwhile, the normalized charge of NaNO₃ solution is almost the same as that of NaCl, indicating that the polyatomic ion may not have a different influence on the transferred charges. Figure 3c presents the average potential of the dielectric surface of the device before and after immersing in solution, which is closely related to surface charges, and Figure S8, Supporting Information, shows the corresponding potential distributions and potential statistics. Although the potential decays obviously after immersing in solution, residual charges remain which are related to the charge output of the device and could be further enhanced by oil triboelectrification.

The influence of pH on the transferred charges is also studied. As shown in Figure 3d, with the increase of pH, the transferred charges first increase and then decrease. The maximum value of transferred charges is 14.73 nC at pH = 7, and the alkaline solution makes the attenuation of the transferred charges more intense. Hydroxide ions, which are regarded to be easily adsorbed on the surface of the dielectric layer, seem more difficult to be swept away by the oil droplet, so the output will decrease.

Figure 3e shows the transferred charges using different dielectric materials as the dielectric layer, with two varied contact areas. According to the triboelectric series,^[16] PTFE has higher affinity to electrons than Kapton, polyethylene terephthalate (PET), and silicone. Thus, the device based on PTFE can reach a higher surface charge density, which results in larger transferred charges during operation of the device. Figure 3f shows the output charges of devices using different types of oils. Compared with other three types of oils, transferred charges by pentadecane can reach a highest value of 33.75 nC with a varied contact area of 16 cm², but pentadecane will swell with some polymers (silicone etc.), damaging surface dielectric layers.

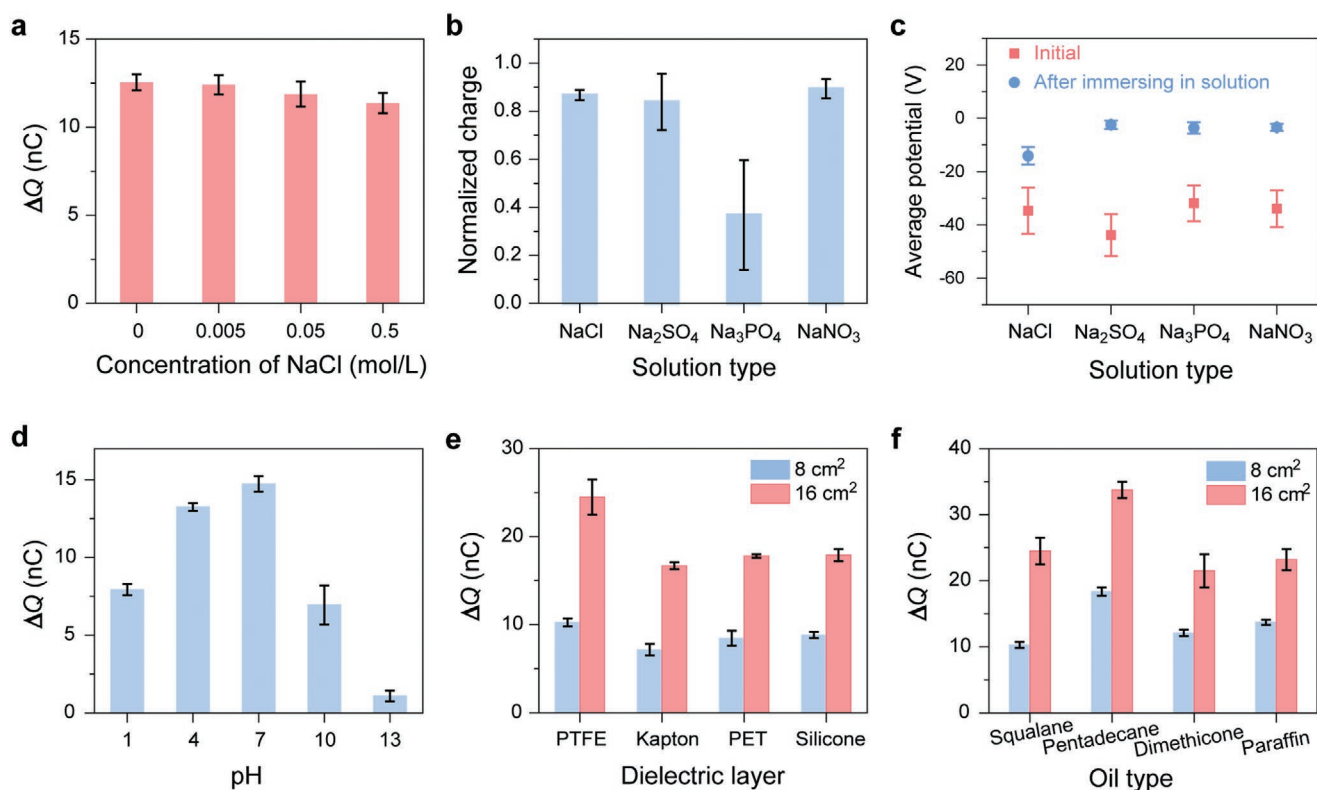


Figure 3. Influence of solutions, dielectric materials and oils. a) Transferred charges with different concentrations of NaCl. b) Normalized charge with different solutions. c) Average potential of the dielectric surface before and after immersing in solutions. d) Transferred charges with different pH. e) Transferred charges with different dielectric materials. f) Transferred charges with different types of oils.

2.4. Devices with Charge Pre-Implantation

To enhance the output of the device, charge pre-implantation to the dielectric layer is adopted based on corona charging (Figure S9a, and details are described in Note S5, Supporting Information). Compared with oil triboelectrification, charge pre-implantation can introduce more charges in the dielectric layer and forming stronger EDL, thus the output charges can be augmented. Meanwhile, the implanted charges can be controlled to be negative or positive. In the experiment, the volume of the oil droplet is 0.9 mL, and the variation of oil–solid contact area is 16 cm². Figure 4a shows the transferred charges of a negative-charge-implanted (NCI) device with multi cycles of squeezing oil droplet. The amount of transferred charges is about -45.8 nC, nearly doubled compared with the device without charge implantation. The drift of charge signal could be caused by slow charge exchange between the surface and water. The output of a positive-charge-implanted (PCI) device is shown in Figure S9b, Supporting Information. To our surprise, the direction of charge transfer is the same as the NCI device, which implies that the oil droplet is sweeping positive charges away during squeezing, and it is counter-intuitive because the positive charges implanted in the dielectric layer should attract anions to the interface.

To further investigate such phenomena, the charge transfer behaviors from the very beginning are compared, as shown in Figure 4b,c. For the NCI device (Figure 4b), the charge transfer

directions of submerging in water (go upward in the figure) and squeezing the oil (go downward in the figure) are opposite. This is compatible with the process shown in Figure 1c. When the device is submerged in water from air, cations will be attracted by the negative charges at the dielectric surface to form the EDL, and electrons should flow to the back electrode. When the oil is squeezed, such cations will be swept away, electrons will flow away from the back electrode due to electrostatic induction. For the PCI device (Figure 4c), the charge transfer directions of submerging in water (go downward in the figure) and squeezing the oil (go downward in the figure) are the same. It seems that anions are attracted to the interface which are not swept away, but cations are swept away by squeezing the oil, implying a more complex charge structure at the interface for the PCI device.

The potential of the dielectric surface is investigated in details to reveal the variation of charge distribution after being submerged in water. First, the NCI device (without oil) is submerged in water (The bare electrode should also be immersed in water to allow charge transfer) and taken out immediately. The potential distributions and potential statistics before and after the operation were measured, as shown in Figure S10a–d, Supporting Information. The absolute value of the surface potential decreases significantly after the operation. The average potential changes from -2626.1 V (Figure S10b, Supporting Information) to -95.2 V (Figure S10d, Supporting Information), and the potential polarity does not change. The

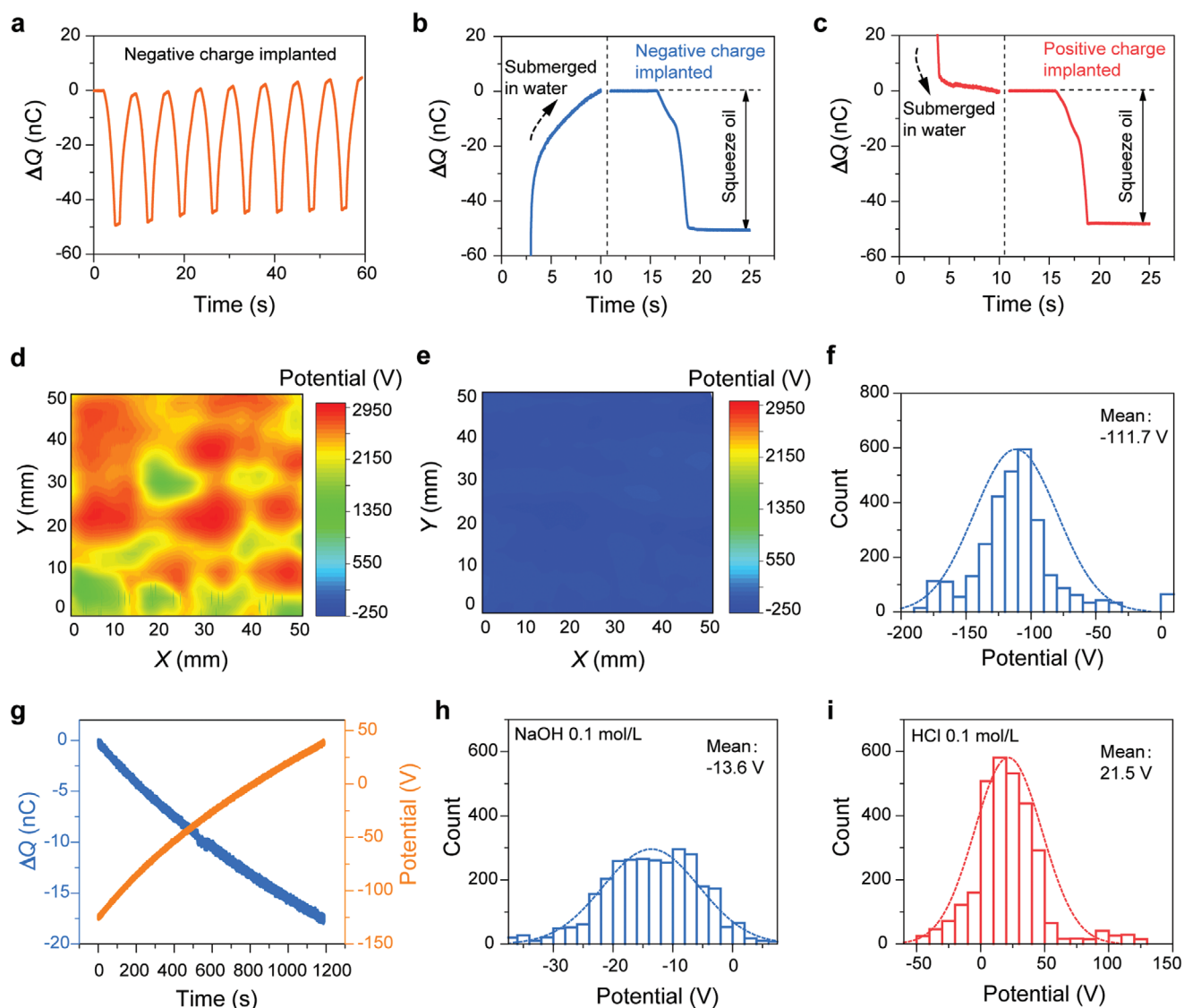


Figure 4. Devices with charge pre-implantation. a) Transferred charges of the NCI device. b) Charge transfer of the NCI device from the beginning. c) Charge transfer of the PCI device from the beginning. d) Initial potential distribution of the PCI device. e, f) Potential distribution (e) and potential statistic (f) of the PCI device after taking out of water (first 1/6 area). g) Real-time monitoring of potential recovery and charge transfer of the PCI device after taking out of water. h) Potential statistic of the PCI device after taking out of NaOH solution (first 1/6 area). i) Potential statistic of the PCI device after taking out of HCl solution (first 1/6 area).

potential after taking out of water could provide some qualitative information on the charge distribution by squeezing oil underwater, because it also removes water away from the dielectric surface. Here, the negative surface potential means that positive screening charges have been removed, which is consistent with previous results. Meanwhile, the surface potential shows fast recovery with time. As shown in Figure S10e,f, Supporting Information, after the device is taken out of water for 720 min, the average potential can recover to -931.8 V, which may be attributed to the evaporation of residual water and ions at the surface. Figure 4d–f shows the potential of PCI device before and after being immersed in water. Compared with the initial potential (Figure 4d), the polarity of the surface potential has changed after being submerged in water

(Figure 4e), and the average potential varies from 2368.1 V (Figure S11, Supporting Information) to -111.7 V (Figure 4f) (Here, only the first 1/6 of the overall potential scanning is used for potential statistic, considering the gradual recovery of surface potential in the process of scanning and the uniformity of surface potential distribution). The results indicate that there are excess negative charges attracted to the PCI dielectric surface, thus exhibits a negative potential to be further screened by cations. This may explain the observed abnormal charge transfer direction for the PCI device. It can be speculated that when immersed in water, negative charges that are more than the positive charges in the dielectric surface are attracted to the interface, which are then screened by cations, and the cations are swept away by the oil during squeezing.

In addition, after the device is placed in air for 10 min, the surface potential of the device restores to positive, with an average value of 0.8 V (Figure S12a,b: Supporting Information). After 720 min, the average potential can recover to about 749.2 V (Figure S12c,d: Supporting Information).

The potential recovery of the PCI device is further real-time monitored by measuring the potential of a sample point and the charge transfer with the bare electrode grounded. As shown in Figure 4g, after being taken out of water, the potential of the sample point returns from -127.1 to 40.5 V after 1200 s, and the corresponding charge transfer is -18.1 nC. For the NCI device, as shown in Figure S13, Supporting Information, the potential of the sample point returns from -97.1 to -430.5 V after 600 s, and the corresponding ΔQ is 34.5 nC. The temperature is found to evidently affect the potential recovery, as shown in Figure S14, Supporting Information. When put in an oven at 60 °C, the average potential of another PCI device quickly recovers from -106.1 V (Figure S14a, Supporting Information) to 559.8 V (Figure S14b, Supporting Information) within 10 min, which is much faster than the device in room temperature. Placing the device in room temperature to 720 min, the average potential can return to 688.8 V (Figure S14c, Supporting Information), which is similar to the first PCI device and seems a saturated state. Comparing the potential of the two devices at different stages, as shown in Figure S14d, Supporting Information, raising the temperature can greatly increase the speed of potential recovery at the early stage. The temperature dependence could further illustrate the residual water and ions on the surface which evaporate faster at a higher temperature.

In order to further reveal the adsorbed charges at the interface, the PCI device is immersed into NaOH and HCl solutions of 0.1 mol L^{-1} respectively, instead of DI water. As shown in Figure 4h, after taking out from the NaOH solution, the potentials of most surface points turn to negative, which is consistent with the situation from DI water. As for the HCl solution, the surface potential is still mainly positive after taking out from the solution (Figure 4i), showing that the potential reversal is suppressed by the HCl solution. Considering the involved ions in DI water and HCl solutions, OH^{-} may be responsible for the potential reversal to negative. In addition, the influence of different concentrations is also studied using NaCl solutions, as shown in Figure S15, Supporting Information. After being submerged in NaCl solutions of 0.005 , 0.05 , and 0.5 mol L^{-1} respectively, the surface potential mainly turns to negative as using DI water, indicating that the concentration has no significant influence. The above results can further support that excess anions (mainly OH^{-}) are attracted by the positive charged dielectric surface of the PCI device underwater, which then attract cations.

2.5. Demonstrations of Energy Harvesting and Self-Powered Sensing

Practical EDL-NG devices are fabricated to demonstrate the energy harvesting performance underwater, as shown in Figure 5a. The device can also be integrated into an array with multiple oil droplets. Figure 5b shows the photograph

of as-fabricated EDL-NGs with single oil drop and oil drop array. Compared with previous reported devices, the EDL-NG can directly work underwater without packaging. Figure 5c–e shows the ΔQ , I_{SC} , and V_{OC} of a single oil drop and an oil drop array EDL-NG. With a motion speed of 1.56 mm s^{-1} , the ΔQ , I_{SC} , and V_{OC} of the single oil drop EDL-NG (volume: 0.9 mL; variation of contact area: 18 cm²) are -28.6 nC, 64.6 nA, and 11.6 V respectively, which are enhanced to -94.7 nC, 107.6 nA and 17.9 V respectively, for the oil droplet array EDL-NG. The curves in Figure 5c,e are presented with the drift base eliminated. The dependence of the output on a resistive load is demonstrated in Figure 5f,g and Figure S16, Supporting Information. A maximum peak power of 59.1 and 157.9 nW can be achieved for the single oil drop and oil drop array EDL-NGs, respectively. Figure 5h shows the charging curve of different capacitors by the EDL-NGs. Under an agitation frequency of 0.17 Hz, the oil drop array EDL-NG can charge a 4.7 μF capacitor to 4.2 V within 300 s. As an intuitive demonstration, the device is shown to directly power light emitting diodes (LEDs) underwater (Figure 5i and Video S2, Supporting Information).

The EDL-NG is also capable of self-powered sensing underwater, with an arch structure. The schematic structure and a photograph of the device are shown in Figure S17, Supporting Information, and Figure 5j, respectively. With 2 mL oil droplet in the device, the relationship between the V_{OC} of the device and the pressure force was tested by a dynamometer, as shown in Figure 5j. The result presents good linearity for sensing force underwater without packaging. A glass rod was used to directly press the device with different magnitudes of force to demonstrate the sensing capability, as shown in Figure 5k and Video S3, Supporting Information. With increased force, the output voltage also rises gradually, consistent with the result shown in Figure 5j. In addition, considering the non-packaged structure, the coupling of oil with water may enable non-contact motion or flow sensing underwater, which senses disturbed water around the oil droplet. Such sensors should be meaningful for underwater robots and equipments.

Although the output is still limited for the device due to the intensity of the EDL, it successfully demonstrates the possibility of using EDL capacitance for energy harvesting with nanogenerators based on oil phase. The working mechanism by driving ions in the EDL is also shown to be achievable for effective energy transmission from external mechanical agitations. Oil is also introduced into the nanogenerator as an important liquid dielectric besides air. Based on the results and characteristics of EDL capacitance, it is reasonable to expect novel EDL devices of high performance with further optimization.

Furthermore, despite existing energy harvesting devices based on water droplets in air, the work here proposed a new system based on multiple phases which allows generalized approach to develop a series of novel devices, and a new conceptual framework which shows that mechanical agitations can be delivered to the charges in the EDL, narrowing the gap between energy harvesting devices and electro-chemical devices. Meanwhile, from the view of application, it is the first nanogenerator device that can work under water without costly packaging. Thus the bare electrified surface

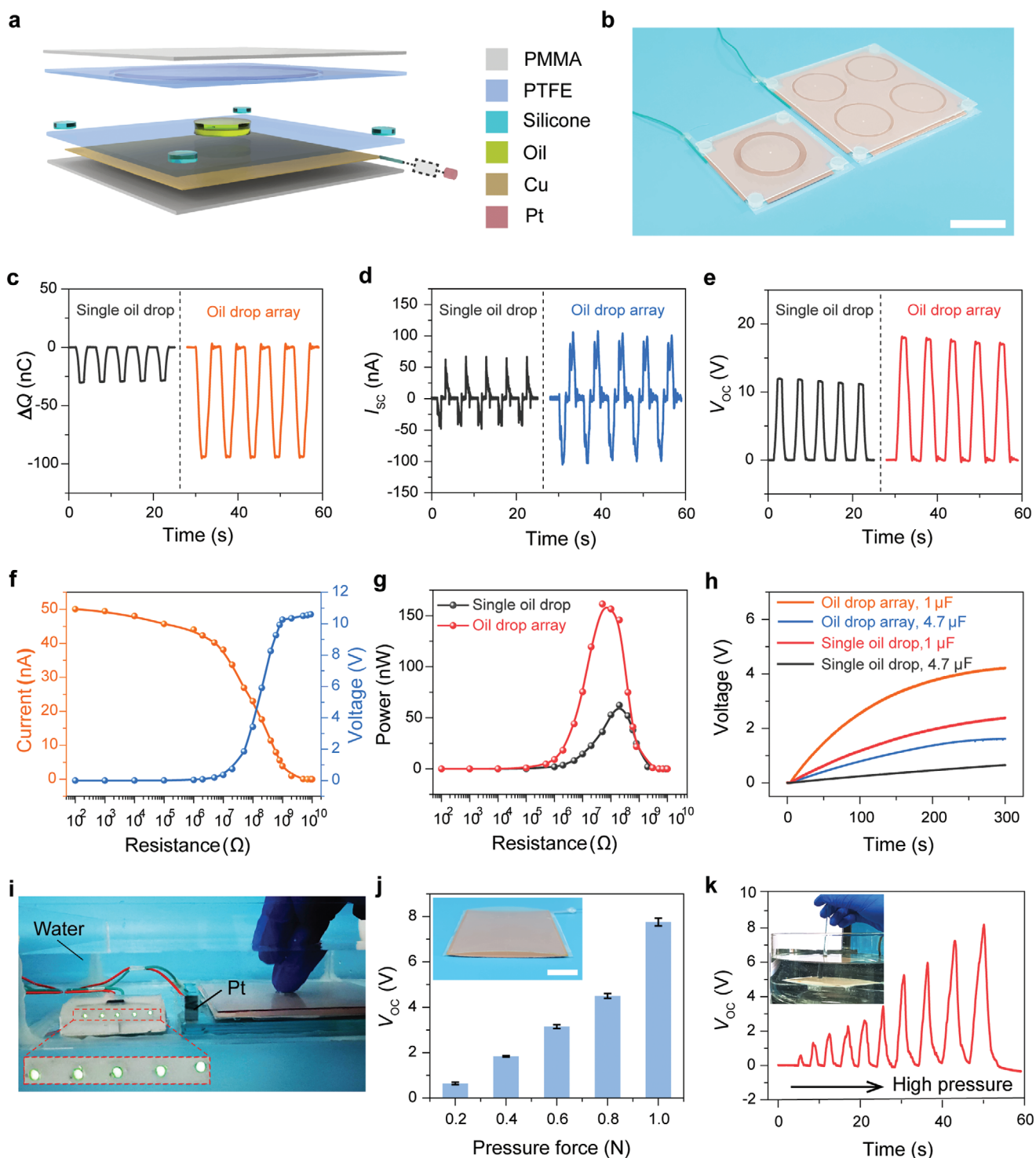


Figure 5. Demonstrations of energy harvesting and self-powered sensing. a) Structure of the practical EDL-NG. b) Photograph of as-fabricated devices with single oil drop and oil drop array. Scale bar, 4 cm. c–e) Transferred charges (c), short-circuit current (d), and open-circuit voltage (e) of the devices. f) Dependence of output current and voltage of the single oil drop device on different resistive loads. g) Dependence of peak power of the devices on different resistive loads. h) Charging performance of the devices for different capacitors. i) Demonstration of directly powering LEDs underwater by the device without packaging. j) Dependence of open-circuit voltage on pressure force. Inset: photograph of the device for sensing. Scale bar, 2 cm. k) Demonstration of pressure sensing underwater. Inset: photograph of pressure sensing underwater.

can directly contact with surrounding aqueous solution, facilitating coupled effect of mechanical agitation and chemical

process, such as mechano-chemistry, electro-chemistry, and electro-catalysis.

3. Conclusion

In this paper, a new mechanism by introducing oil phase into water–solid interface is demonstrated to enable a nanogenerator based on EDL. The EDL-NG works via squeezing and releasing the oil droplet in water environment. Charge transfer can be generated in the back electrode accompanying the spread and retraction of the oil droplet and the movement of oil–water–solid three-phase line. The charge transfer is mainly caused by the effect that the oil phase sweeps away charges near the dielectric surface in the EDL based on the discrepancy of EDL between water–solid and oil–solid interfaces. Experimental results show that the device can be applied in various aqueous environment effectively, and through charge pre-implantation in the dielectric surface, the performance can be further enhanced. Under water environment, the device can work directly for energy harvesting and self-powered sensing without costly packaging. The EDL-NG reveals that the charges in the EDL can be effectively driven for energy harvesting with oil phase, narrowing the gap between energy harvesting devices and electro-chemical devices. Based on the new working mode relying on EDL, novel nanogenerators adapt to severe environment even underwater with low friction and wear can be developed, toward new nanogenerators with overwhelming performance for practical applications ranging from blue energy harvesting to electro-catalysis.

4. Experimental Section

Fabrication of the EDL-NG: To fabricate the proof-of-principle device, for the lower plate, an acrylic substrate was cut by a laser cutter (PLS6.75) with dimensions of 50 mm × 50 mm × 2 mm. A copper electrode with a thickness of 30 μm was adhered to the substrate as the back electrode. Then a piece of PTFE film (ASF-110 FR, thickness: 80 μm) was attached on the copper electrode as the dielectric layer. Another piece of PTFE film was attached on the opposite side to wrap the substrate for ensuring water tightness of the back electrode, which is neglected in schematic structure figures. A Pt electrode, with dimensions of 15 mm × 5 mm × 0.1 mm, was connected to the copper electrode as the bare electrode. For the upper plate, a PTFE film was attached on a glass substrate (60 mm × 60 mm × 3 mm), and an annular cutting was made at the center of the PTFE film with an inner diameter of 30 mm, which can locate the oil drop injected into the gap between the upper and lower plates by a glass syringe (5 mL).

To fabricate the single oil drop EDL-NG, two pieces of acrylic substrates were cut by the laser cutter with dimensions of 75 mm × 75 mm × 1 mm. PTFE films and copper electrodes were attached to the substrates similar to the proof-of-principle EDL-NG. Then the bare electrode was connected and the oil drop was injected. The upper plate and the lower plate were connected by silicone spacers (Ecoflex 00–30), which were casted by an acrylic round trough (diameter: 8 mm, height: 2 mm) with the base and the curing agent mixed in 1:1 weight ratio, and cured at room temperature for at least 4 h. For oil drop array EDL-NG, two pieces of acrylic substrates were cut by the laser cutter with dimensions of 120 mm × 120 mm × 1 mm. Following fabrication processes were similar as the single oil drop EDL-NG, except that four annular cuttings were made in the PTFE film with four oil drops injected.

Fabrication of the Arch Device for Sensing: Two pieces of polycarbonate (PC) plates were cut as substrates by the laser cutter with dimensions of 80 mm × 80 mm × 0.3 mm. The plates were made into arches by single-sided heating using hot air gun (150 °C, 5 min). For the lower plate, a copper electrode with a thickness of 30 μm was adhered to a substrate, which was then wrapped by PTFE films. A Pt electrode, with dimensions of 15 mm × 5 mm × 0.1 mm, was connected to the copper electrode as

the bare electrode. For the upper plate, another substrate was attached with PTFE film. The upper and lower plates were assembled together using PTFE tape with oil injected.

Characterization of the Device: The transferred charges, the open-circuit voltage, the current, and the voltage of capacitors were measured by an electrometer (Keithley 6514). The surface potential of the device was measured by an electrostatic voltmeter (Trek 347). A 2D displacement platform (Zolix KSA100-11-X for each dimension) was used for scanning in the potential measurement. A source meter (Keithley 2410) was adopted as the voltage source to inject charges for testing capacitance. A high-voltage source (ET2673A) was used for charge implantation. In most performance tests of the device, the upper plate was fixed on a linear motor (DGS-1204) by a glass bracket to move up and down. The water environment is prepared in a glass container.

Supporting Information

Supporting Information is available from the Wiley Online Library or from the author.

Acknowledgements

The research was supported by the National Natural Science Foundation of China (No. 51605033, 51735001), the Key Research Program of Frontier Sciences, CAS (ZDBS-LY-DQC025), and Youth Innovation Promotion Association, CAS (No. 2019170).

Conflict of Interest

The authors declare no conflict of interest.

Author Contributions

H.F.Q. and L.X. contributed equally to this work. L.X. and Z.L.W. conceived the idea and guided the project. L.X. designed the experiments. H.Q. fabricated the device. H.Q. did the experiments. K.H. and Y.F. participated in the experiments. H.Q., L.X., Z.L.W., S.L., F.Z., and H.W. analyzed the data. H.Q., L.X., Z.L.W., S.L., F.Z., K.D., and H.W. wrote and revised the manuscript.

Data Availability Statement

The data that support the findings of this study are available from the corresponding author upon reasonable request.

Keywords

electric double layers, energy harvesting, nanogenerators, oils, underwater

Received: November 16, 2021

Revised: January 10, 2022

Published online:

[1] a) E. Borgia, *Comput. Commun.* **2014**, *54*, 1; b) S. Wang, J. Xu, W. Wang, G. N. Wang, R. Rastak, F. Molina-Lopez, J. W. Chung, S. Niu, V. R. Feig, J. Lopez, T. Lei, S. K. Kwon, Y. Kim, A. M. Foudeh, A. Ehrlich, A. Gasperini, Y. Yun, B. Murmann, J. B. Tok, Z. Bao,

- Nature* **2018**, 555, 83; c) Q. Zheng, Y. Zou, Y. L. Zhang, Z. Liu, B. J. Shi, X. X. Wang, Y. M. Jin, H. Ouyang, Z. Li, Z. L. Wang, *Sci. Adv.* **2016**, 2, 1501478; d) J. Wang, S. Li, F. Yi, Y. Zi, J. Lin, X. Wang, Y. Xu, Z. L. Wang, *Nat. Commun.* **2016**, 7, 12744; e) Z. L. Wang, *Mater. Today* **2017**, 20, 74.
- [2] a) F.-R. Fan, Z.-Q. Tian, Z. L. Wang, *Nano Energy* **2012**, 1, 328; b) Z. L. Wang, *Rep. Prog. Phys.* **2021**, 84, 096502; c) Y. Shi, F. Wang, J. Tian, S. Li, E. Fu, J. Nie, R. Lei, Y. Ding, X. Chen, Z. L. Wang, *Sci. Adv.* **2021**, 7, eabe2943; d) Q. Zhou, J. Pan, S. Deng, F. Xia, T. Kim, *Adv. Mater.* **2021**, 33, 2008276; e) X. Yang, L. Xu, P. Lin, W. Zhong, Y. Bai, J. Luo, J. Chen, Z. L. Wang, *Nano Energy* **2019**, 60, 404.
- [3] a) J. Bae, J. Lee, S. Kim, J. Ha, B. S. Lee, Y. Park, C. Choong, J. B. Kim, Z. L. Wang, H. Y. Kim, J. J. Park, U. I. Chung, *Nat. Commun.* **2014**, 5, 4929; b) Z. H. Lin, G. Cheng, S. Lee, K. C. Pradel, Z. L. Wang, *Adv. Mater.* **2014**, 26, 4690; c) L. Xu, Y. Pang, C. Zhang, T. Jiang, X. Chen, J. Luo, W. Tang, X. Cao, Z. L. Wang, *Nano Energy* **2017**, 31, 351; d) L. Xu, T. Jiang, P. Lin, J. J. Shao, C. He, W. Zhong, X. Y. Chen, Z. L. Wang, *ACS Nano* **2018**, 12, 1849; e) Y. Bai, L. Xu, S. Lin, J. Luo, H. Qin, K. Han, Z. L. Wang, *Adv. Energy Mater.* **2020**, 10, 2000605; f) H. Wang, L. Xu, Y. Bai, Z. L. Wang, *Nat. Commun.* **2020**, 11, 4203; g) F. Xi, Y. Pang, W. Li, T. Jiang, L. Zhang, T. Guo, G. Liu, C. Zhang, Z. L. Wang, *Nano Energy* **2017**, 37, 168; h) G. Yao, L. Xu, X. Cheng, Y. Li, X. Huang, W. Guo, S. Liu, Z. L. Wang, H. Wu, *Adv. Funct. Mater.* **2019**, 30, 1907312.
- [4] Z. L. Wang, A. C. Wang, *Mater. Today* **2019**, 30, 34.
- [5] S. Niu, Z. L. Wang, *Nano Energy* **2015**, 14, 161.
- [6] a) S. Wang, Y. Xie, S. Niu, L. Lin, C. Liu, Y. S. Zhou, Z. L. Wang, *Adv. Mater.* **2014**, 26, 6720; b) J. Wang, C. Wu, Y. Dai, Z. Zhao, A. Wang, T. Zhang, Z. L. Wang, *Nat. Commun.* **2017**, 8, 88.
- [7] L. Xu, T. Z. Bu, X. D. Yang, C. Zhang, Z. L. Wang, *Nano Energy* **2018**, 49, 625.
- [8] V. Nguyen, R. Yang, *Nano Energy* **2013**, 2, 604.
- [9] Y. Zou, P. Tan, B. Shi, H. Ouyang, D. Jiang, Z. Liu, H. Li, M. Yu, C. Wang, X. Qu, L. Zhao, Y. Fan, Z. L. Wang, Z. Li, *Nat. Commun.* **2019**, 10, 2695.
- [10] W. Xu, H. Zheng, Y. Liu, X. Zhou, C. Zhang, Y. Song, X. Deng, M. Leung, Z. Yang, R. X. Xu, Z. L. Wang, X. C. Zeng, Z. Wang, *Nature* **2020**, 578, 392.
- [11] a) L. G. Gouy, *J. Phys. Theory Appl.* **1910**, 9, 457; b) D. L. Chapman, *Philos. Mag.* **1913**, 25, 475; c) O. Stern, *Z. Electrochem.* **1924**, 30, 508; d) S. Lin, L. Xu, A. C. Wang, Z. L. Wang, *Nat. Commun.* **2020**, 11, 399; e) J. R. Miller, P. Simon, *Science* **2008**, 321, 651.
- [12] P. Simon, Y. Gogotsi, *Nat. Mater.* **2008**, 7, 845.
- [13] D. C. Grahame, *Chem. Rev.* **1947**, 41, 441.
- [14] a) J. Lyklema, *Adv. Colloid Interfaces* **1968**, 2, 67; b) A. Kitahara, *Prog. Org. Coat.* **1973**, 2, 81; c) A. Kitahara, A. Watanabe, *Electrical Phenomena at Interfaces*, Dekker, New York, USA **1984**.
- [15] Y. S. Zhou, Y. Liu, G. Zhu, Z. H. Lin, C. Pan, Q. Jing, Z. L. Wang, *Nano Lett.* **2013**, 13, 2771.
- [16] D. K. Davies, *J. Phys. D: Appl. Phys.* **1969**, 2, 1533.